Proceedings of Global Power and Propulsion Society
ISSN-Nr: 2504-4400
GPPS Hong Kong 2023
October 17-19, 2023
www.gpps.global

GPPS-TC-2023-0193

Multi-fidelity aerodynamic performance modeling of supercritical carbon dioxide compressor

Can Ma[1,2]
[1]Science and Technology on Thermal Energy and Power Laboratory
[2]Wuhan Second Ship Design and Research Institute
macan1234@sina.com
Wuhan, Hubei, China

Jinlan Gou[1,2]
[1]Science and Technology on Thermal Energy and Power Laboratory
[2]Wuhan Second Ship Design and Research Institute
gjl12@tsinghua.org.cn
Wuhan, Hubei, China

Xingsheng Lao[1,2]
[1]Science and Technology on Thermal Energy and Power Laboratory
[2]Wuhan Second Ship Design and Research Institute
enginefluid@163.com
Wuhan, Hubei, China

Kelong Zhang[1,2]
[1]Science and Technology on Thermal Energy and Power Laboratory
[2]Wuhan Second Ship Design and Research Institute
luckyzkl@163.com
Wuhan, Hubei, China

Wei Wang[1,2]
[1]Science and Technology on Thermal Energy and Power Laboratory
[2]Wuhan Second Ship Design and Research Institute
wangweirndl@sina.com
Wuhan, Hubei, China

ABSTRACT

Fast and accurate prediction of compressor aerodynamic performance is required in the system design and analysis of the supercritical carbon dioxide(S-CO2) power cycle. However, the S-CO2 compressor typically operates at an inlet fluid state close to the fluid critical point for optimal cycle efficiency. As the fluid parameters vary significantly near the critical point, accurate compressor modeling is more challenging with current meanline models, considering lack of adequate experimental data to validate various empirical correlations. This work proposed a multi-fidelity model for the aerodynamic performance prediction of the S-CO2 compressor, which enhances the meanline model with limited reliable experimental data or high-fidelity numerical data. The advantage of low cost with the meanline model is retained in the current multi-fidelity model, while a cheap surrogate model is constructed to improve the accuracy. The model is applied to the aerodynamic performance prediction of typical S-CO2 compressor cases.

INTRODUCTION

The supercritical carbon dioxide (S-CO2) Brayton cycle is a promising option for future nuclear power generation. Due to the high density of S-CO2, the size of compressor and turbine is much smaller than the steam-based turbomachinery, leading to a more compact power system with high thermal efficiency and reduced manufacturing cost. In recent years, more and more investigations on the supercritical carbon dioxide power cycle are carried out (Brun et al., 2017; Dostal et al., 2006; Reyes-Belmonte, 2016; Yari, 2012). Compressor is the critical component in the S-CO2 Brayton cycle system. One of the reasons for a high thermal efficiency of the S-CO2 cycle comes from the fact that the compression work is significantly reduced as the compressor inlet state approaches the critical point of CO2. However, a compressor operating near the fluid critical point is more vulnerable to flow instabilities and care must be taken in designing the S-CO2 compressor.

Due to the high working pressure and small size of the compressor, it is difficult to obtain any detailed flow measurement and the experimental results are limited to total operation performance such as mass flow rate and pressure ratio. In recent years, computational fluid dynamics (CFD) simulations are used to explore the flow details in the S-CO2 compressor. Pecnik et al. (2012) performed steady flow simulation of the impeller of an S-CO2 radial compressor by

solving the Reynolds Averaged Navier-Stokes (RANS) equations. Lettieri et al. (2014) performed aerodynamic design and steady RANS simulation of an S-CO2 compressor stage. Ameli et al. (2016) performed steady RANS simulation of an S-CO2 compressor impeller. Behafarid and Podowski (2016) performed unsteady direct numerical simulation (DNS) of the impeller of an S-CO2 radial compressor. The authors (Ma et al., 2018) carried out unsteady RANS simulation of an S-CO2 radial compressor stage consisting of an impeller and a wedge diffuser. Romei et al. (2022) performed RANS simulation of a centrifugal compressor with inlet guide vanes.

As the CFD simulation is time-consuming, the meanline model is also used for the performance prediction of the S-CO2 compressor (Lee et al., 2012; Liu et al., 2018; Chen et al., 2019; Shao et al., 2020). However, the accuracy of the empirical correlations in the meanline models have not been systematically validated against S-CO2 compressor, partly due to lack of experimental data.

In this work, a multi-fidelity model of S-CO2 compressor is developed based on the co-Kriging method. The low-fidelity model is constructed with the simulation results of the meanline model, limited number of CFD results are incorporated as high-fidelity data. The multi-fidelity model shows similar accuracy with the CFD model in predicting the performance characteristics and the computational cost is reduced.

NUMERICAL METHODS

A 100 kW-class single-stage radial compressor stage consisting of an impeller and a wedge diffuser is investigated in this work. The unsteady flow analysis of the compressor has been performed in previous work (Ma et al., 2018). The impeller tip gap is 0.2 mm, which corresponds to 17% of the blade height at the impeller exit. The impeller blade number is 12 with half of the blade being split blade. The diffuser vane number is 18. The design parameters of the compressor are shown in Table 1. The static pressure and temperature at the inlet is close to the fluid critical point (7.38MPa, 304.13K). The total pressure and temperature are set as the inlet boundary conditions and they are assumed to be constant. The geometric model of the compressor stage is shown in Figure 1.

Table 1 Design parameters of the S-CO2 radial compressor

Design parameters	
p_{t0} [MPa]	7.69
p_0 [MPa]	7.55
T_{t0} [K]	308.15
T_0 [K]	307.32
p_2 [MPa]	13.5
N [rpm]	4×10^4
N_s [-]	0.38

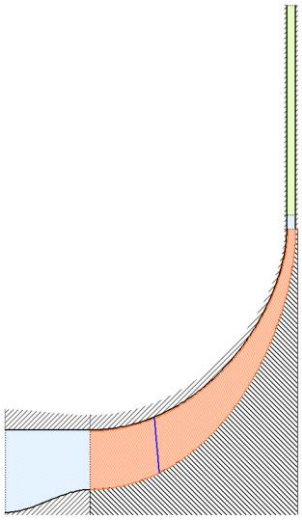

Figure 1 Meridional view of the S-CO2 radial compressor

Meanline model

The meanline modeling is carried out with the commercial software Concepts NREC COMPAL. The flow at the exit of the compressor impeller is calculated with the two-zone model, which divides the flow into primary and secondary zones (Japikse, 1996). The flow in the primary zone is assumed to have reached the impeller exit plane through an

isentropic process. All the loss inside the impeller passage is assumed to be concentrated inside the secondary zone. One of the key parameters in the two-zone model is the diffusion ratio, the ratio of impeller inlet tip relative velocity to primary zone relative velocity at the impeller exit. Three options are chosen for the diffusion ratio modelling in this work: the Two-Element-In-Series model, the backbone curve model and the hybrid function model. All the modelling options rely on empirical correlations. The Two-Element-In-Series model divides the impeller into two elements in series, with the first element a diffuser or nozzle and the second element a diffuser, whose performance are specified according to users' experience. The backbone curve model first calculates the ideal isentropic diffusion ratio and then relates the actual diffusion ratio to the ideal diffusion ratio with an empirical curve. The hybrid function model first calculates the diffusion ratio with the backbone curve and then corrects the performance of the two elements to account for off-design conditions as well as the design condition.

Table 2 Diffusion ratio modeling methods

Meanline model	Diffusion ratio modeling methods
A	Two-Element-In-Series
B	backbone curve
C	hybrid function

CFD model

The computational grid is generated using the commercial software NUMECA/AutoGrid. The grid for each blade passage is shown in Figure 2. The number of grid points for the impeller is 1.39M for one main blade passage and one split blade passage. The vane passage is discretized with 1.08M grid points. The wall y^+ is below 1, which enables the use of a wall-resolved turbulence model. In addition to the baseline mesh with 2.5M grid points, the simulation has been performed with a coarse mesh with 0.6M grid points and a fine mesh with 10M grid points. As shown in Table 3, compared with the fine mesh, the discrepancy of the result with the baseline mesh in the mass flow is 0.1% and the efficiency is 0.07%, which is acceptable for performance parameters. Therefore, the baseline mesh is adopted for the simulation.

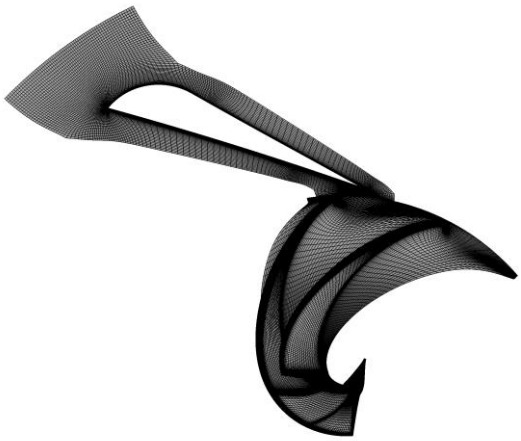

Figure 2 Computational grid for the mixing-plane flow simulation

Table 3 Simulation result with various grids

Mesh	Grid points count	Mass flow rate (kg/s)	Isentropic efficiency (%)
Coarse	0.6×10^6	5.309	79.54
Baseline	2.5×10^6	5.111	78.79
Fine	1.0×10^7	5.105	78.72

The three-dimensional steady Reynolds Averaged Navier-Stokes (RANS) equations are solved using the commercial software NUMECA/Fine-Turbo. The fluid properties of S-CO2 are based on the National Institute of Standards and Technology (NIST) database. When generating the fluid property tables, clustered points are set near the saturation lines to increase the accuracy. The two-equation k-ω SST model is used for the turbulence modeling. The computational grid consists of one main and split blade passage for the impeller as well as one blade passage for the diffuser. The mixing-plane model is used for the data exchange on the impeller-diffuser interface, where the circumferentially averaged flow variables are specified as the boundary condition on the other side.

Multi-fidelity model

The multi-fidelity model in this work is constructed based on the co-Kriging method developed by Su and co-authors (Zhang et al., 2019), which has been applied to the performance prediction and optimization of a film cooling hole. The stochastic process for the low-fidelity prediction is

$$Y_l(\mathbf{x}) = \mu_l + Z_l(\mathbf{x}) \qquad (1)$$

where $\mathbf{x}$ is the sampling point with m dimensions, μ_l denotes the mean value and Z_l denotes a stochastic process which follows Gaussian distribution. The covariance of the stochastic processes for two different sampling points is given by

$$Cov\left(Z_l(\mathbf{x}^i), Z_l(\mathbf{x}^j)\right) = \sigma^2 R(\mathbf{x}^i, \mathbf{x}^j) \quad (2)$$

where σ^2 denotes the variance of the model and R denotes the the correlation coefficient between two sampling points $\mathbf{x}^i$ and $\mathbf{x}^j$. The correlation coefficient is defined with Gaussian correlation functions

$$R(\mathbf{x}^i, \mathbf{x}^j) = \prod_{k=1}^{m} \exp\left(-\theta_{ck} \left\| \mathbf{x}_k^i - \mathbf{x}_k^j \right\|^2\right) \quad (3)$$

where θ_{ck} (k = 1, 2, …, m) can be obtained by solving the maximum likelihood function of combined Gaussian distribution.

Similar to the low-fidelity prediction, the stochastic process for the prediction of a high-fidelity sampling point consists two parts

$$Y_h(\mathbf{x}) = \mu_h + Z_h(\mathbf{x}) \qquad (4)$$

with the co-Kriging method, $Z_h(\mathbf{x})$ is defined as

$$Z_h(\mathbf{x}) = \rho Z_l(\mathbf{x}) + Z_d(\mathbf{x}) \qquad (5)$$

where ρ is a scalar and $Z_d(\mathbf{x})$ is another stochastic process. The complex covariance matrix composed of the low fidelity and the high-fidelity sampling points is defined as

$$\mathbf{C} = \begin{pmatrix} \sigma_l^2 R_l(\mathbf{x}_l, \mathbf{x}_l) & \rho\sigma_l^2 R_l(\mathbf{x}_l, \mathbf{x}_h) \\ \rho\sigma_l^2 R_l(\mathbf{x}_h, \mathbf{x}_l) & \rho^2\sigma_l^2 R_l(\mathbf{x}_h, \mathbf{x}_h) + \sigma_d^2 R_d(\mathbf{x}_h, \mathbf{x}_h) \end{pmatrix} \qquad (6)$$

The high fidelity prediction can be written as

$$\hat{y}(\mathbf{x}) = \hat{\mu} + \mathbf{c}^{\mathrm{T}}\mathbf{C}^{-1}(\mathbf{y} - \mathbf{1}\hat{\mu}) \qquad (7)$$

where

$$\hat{\mu} = \mathbf{1}^{\mathrm{T}}\mathbf{C}^{-1}\mathbf{y} / \mathbf{1}^{\mathrm{T}}\mathbf{C}^{-1}\mathbf{1} \qquad (8)$$

and

$$\mathbf{c} = \begin{pmatrix} \hat{\rho}\hat{\sigma}_l^2 R_l(\mathbf{x}_l, \mathbf{x}) \\ \hat{\rho}\hat{\sigma}_l^2 R_l(\mathbf{x}_h, \mathbf{x}) + \hat{\sigma}_d^2 R_d(\mathbf{x}_h, \mathbf{x}) \end{pmatrix} \qquad (9)$$

The low-fidelity model is constructed with the simulation results of the meanline model, which provides the trend. The high-fidelity data is obtained with CFD, which is more expensive in computational cost than the meanline model. The multi-fidelity model is constructed with the low-fidelity model and limited high-fidelity data. In this work, five CFD points on the performance characteristic curve are used as the high-fidelity data to construct the multi-fidelity model.

RESULTS AND DISCUSSION

The performance characteristics of the compressor at design speed simulated with CFD model and various meanline models are shown in Figure 3. The mass flow rate is normalized by the value at design point. According to the CFD results, the isentropic efficiency of the compressor varies less than 1% from 80% to 100% design mass flow, with the peak efficiency 79.2% observed at approximately 93% design mass flow. With a further increase of the mass flow rate, the efficiency begins to drop obviously. For the meanline model A and B results, the peak efficiency is observed at

approximately 80% design mass flow and the efficiency then shows a more gradual drop as the mass flow increases. For the meanline model C results, however, the efficiency decrease as the mass flow increases within the whole simulated mass flow range. For the pressure ratio, the CFD results and the meanline model results shows the same trend that the pressure ratio decreases as the mass flow rate increases. In general, the meanline model results show obvious discrepancy with the CFD results for both the efficiency and the pressure ratio. Although the computational cost is low, the accuracy of the meanline model heavily relies on the accuracy of the empirical correlations, which are generally based on experimental data with air compressors. As the experimental data of the S-CO2 compressor are limited, the accuracy of the meanline model in the existing commercial software has not been systematically verified. Compared with the meanline model, the three-dimensional CFD is based on more detailed geometric model and less simplified numerical model. Therefore, the CFD result is adopted as the high-fidelity result in this work.

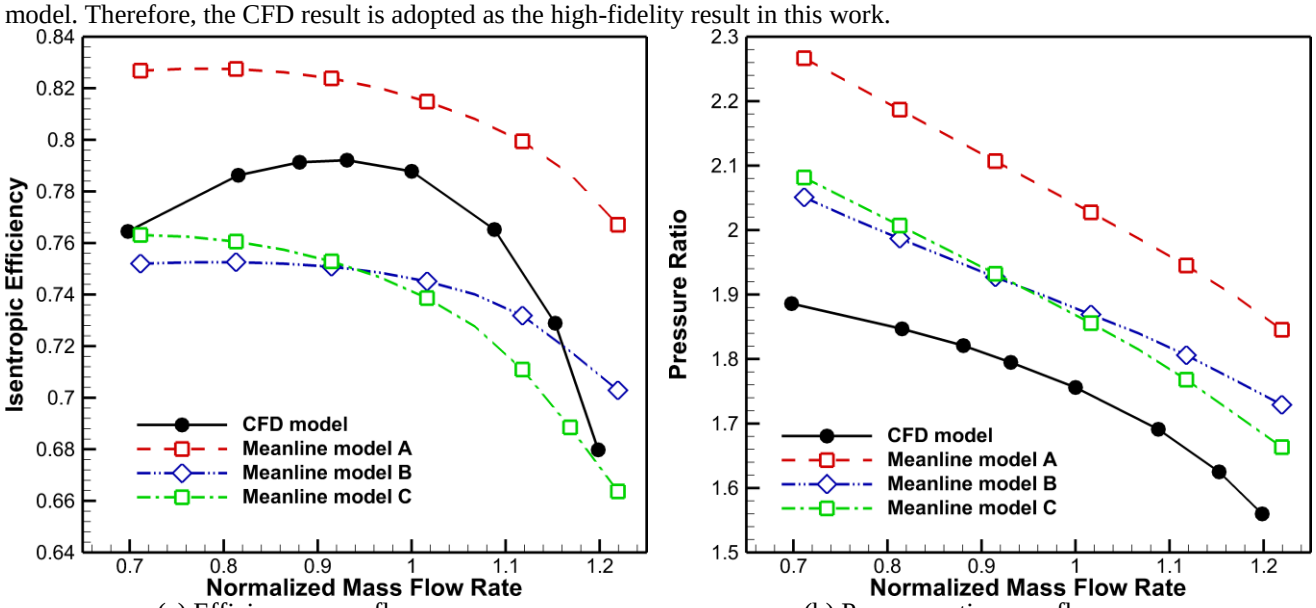

(a) Efficiency-mass flow curve (b) Pressure ratio-mass flow curve

Figure 3 Performance characteristics of compressor simulated with CFD model and various meanline models

The performance characteristics of the compressor at design speed with multi-fidelity model based on meanline model A are shown in Figure 4. The maximum efficiency discrepancy of meanline model A is 10 points while the maximum pressure ratio discrepancy is 20%. The multi-fidelity model shows good agreement with the CFD results and the maximum efficiency discrepancy is about 0.8 points while the maximum pressure ratio discrepancy is about 1.0%.

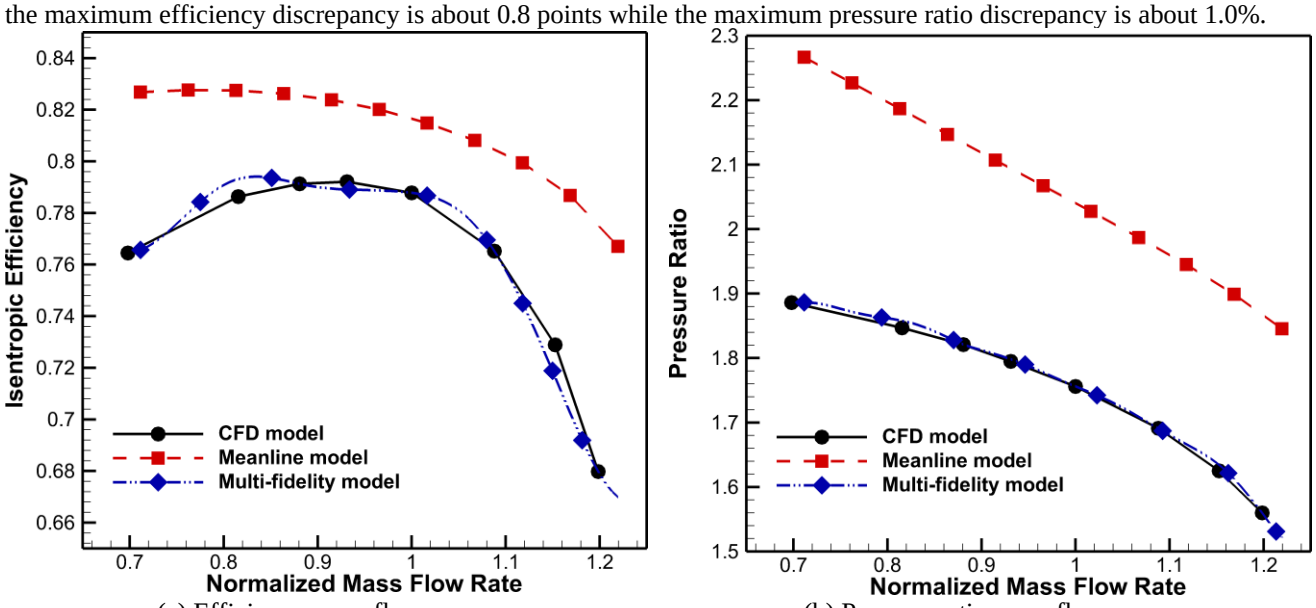

(a) Efficiency-mass flow curve (b) Pressure ratio-mass flow curve

Figure 4 Performance characteristics of compressor simulated with multi-fidelity model based on meanline model A

The performance characteristics of the compressor at design speed with multi-fidelity model based on meanline model B and C are shown in Figure 5 and Figure 6. Similarly, the multi-fidelity models show good agreement with the CFD results, despite the meanline model results are quite different.

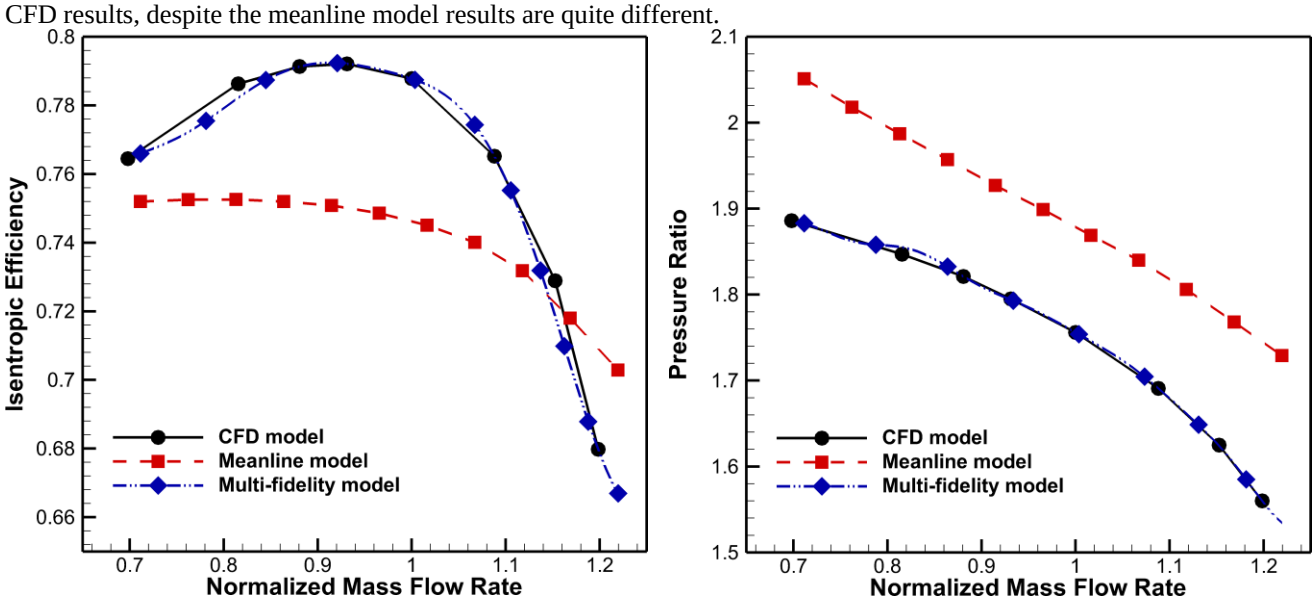

(a) Efficiency-mass flow curve (b) Pressure ratio-mass flow curve

Figure 5 Performance characteristics of compressor simulated with multi-fidelity model based on meanline model B

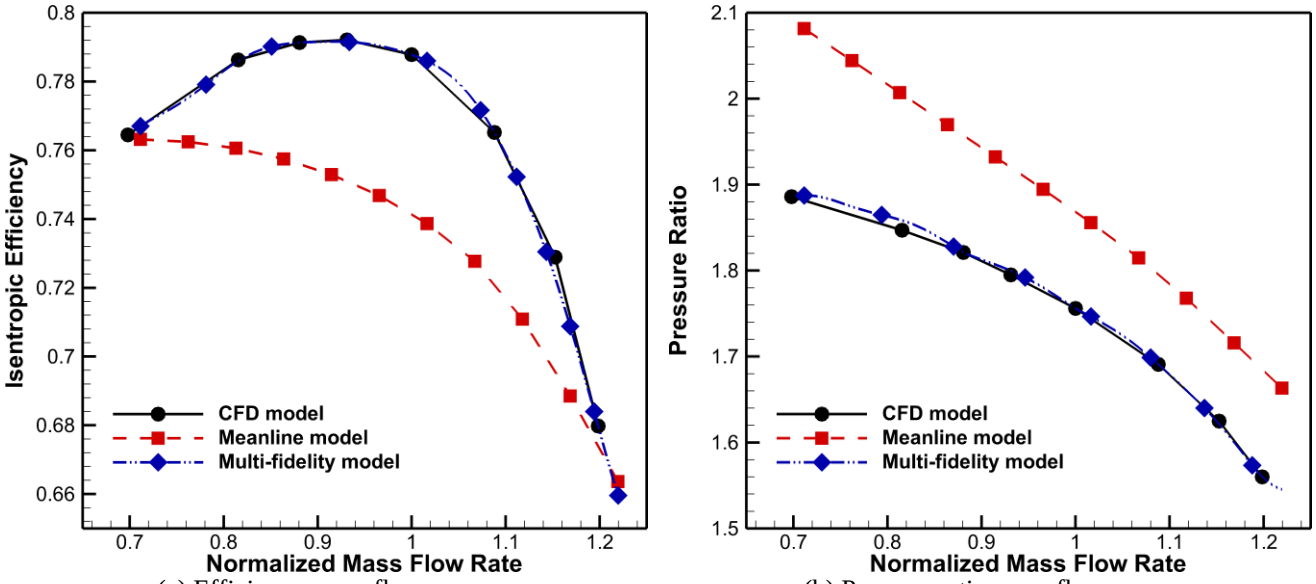

(a) Efficiency-mass flow curve (b) Pressure ratio-mass flow curve

Figure 6 Performance characteristics of compressor simulated with multi-fidelity model based on meanline model C

The performance characteristics of the compressor at design speed with various multi-fidelity models are shown in Figure 7. With different meanline models as the basis, the multi-fidelity model results show some variations. The maximum efficiency discrepancy is about 1.2 points while the maximum pressure ratio discrepancy is about 1.2%. In general, the multi-fidelity model compares well with the CFD results. The computational cost of the meanline model is almost negligible compared to the CFD results. Therefore, the computational cost of the multi-fidelity model largely depends on how many high-fidelity simulations are performed to construct the model. In this work, 5 CFD points are used as the high-fidelity data to construct the multi-fidelity model as well as 11 meanline points as the low-fidelity data. Therefore, the computational cost saving of the multi-fidelity model compared to the high-fidelity model is about 55%.

The meanline model is computationally cheap and suitable for predicting the performance trend, but the accuracy of a single point heavily relies on verified empirical correlations. The three-dimensional CFD is computationally expensive but based on more detailed geometry and numerical model and is thus more reliable than the meanline model for

turbomachinery with less experimental data. The multi-fidelity model combines the advantages of the meanline model and the CFD method, with the accuracy comparable to the CFD method and the computational cost obviously reduced when a series of performance predictions are needed, such as in the design optimization.

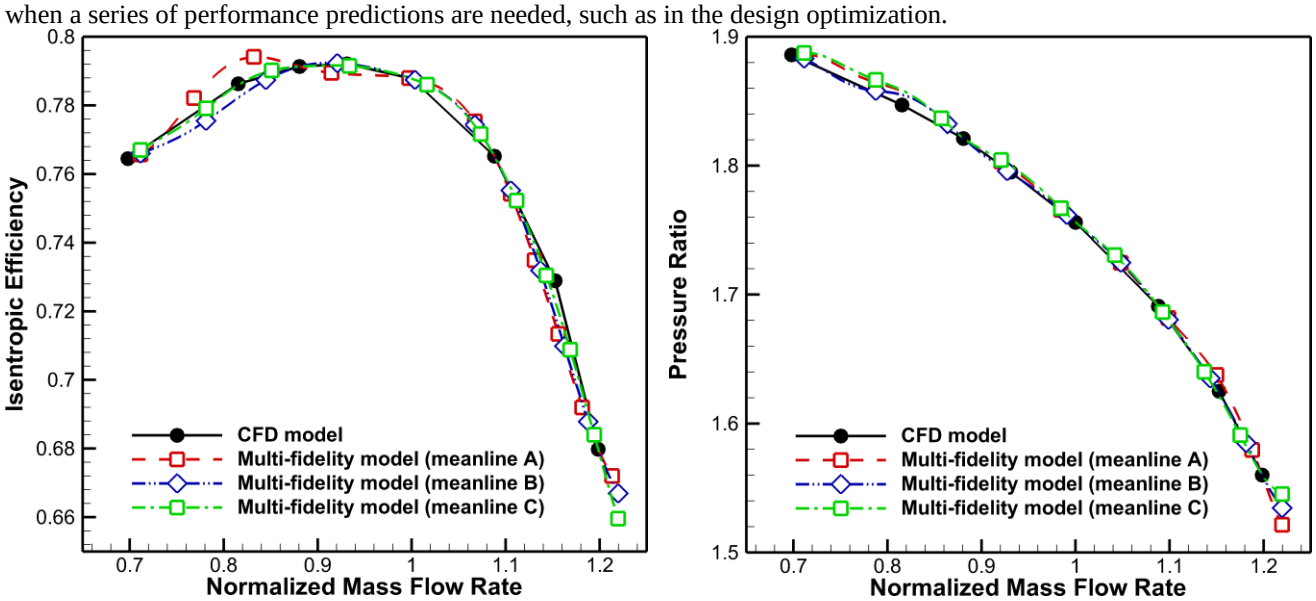

(a) Efficiency-mass flow curve (b) Pressure ratio-mass flow curve

Figure 7 Performance characteristics of compressor simulated with CFD model and various multi-fidelity models

CONCLUSIONS

A multi-fidelity model is applied to the performance prediction of the S-CO2 compressor. The low-fidelity model is constructed with the simulation results of the meanline model, with empirical correlations not systematically validated against S-CO2 compressor. Three meanline models with diffusion ratio modeling methods are used to simulate the compressor characteristics and the efficiency and pressure ratio results show obvious discrepancy compared with CFD results. Five CFD points on the performance characteristics are used as high-fidelity data to constructed the multi-fidelity model based on various low-fidelity models. In general, the multi-fidelity model compares well with the CFD results, despite the meanline model results are quite different. Comparing the multi-fidelity model with the CFD results, the maximum efficiency discrepancy is about 0.8 points while the maximum pressure ratio discrepancy is about 1.0%. Therefore, the multi-fidelity model shows similar accuracy with the CFD model in predicting the performance characteristics and the computational cost is reduced.

NOMENCLATURE

Symbols

h	Specific enthalpy
h_0	Total specific enthalpy
N	Impeller rotating speed
N_s	Specific speed $\dfrac{2\pi NQ^{0.5}}{60\left(h_{2s}-h_{00}\right)^{0.75}}$
p	Pressure
p_0	Total pressure
Q	Volume flow rate
T	Temperature
T_0	Total temperature

Subscripts

0	Impeller inlet
1	Impeller outlet
2	Diffuser outlet
s	Isentropic state

Abbreviations

S-CO2	Supercritical Carbon Dioxide

CFD	Computational Fluid Dynamics
RANS	Reynolds Averaged Navier-Stokes
NIST	National Institute of Standards and Technology

ACKNOWLEDGMENTS

This work is partly supported by the grant from the National Natural Science Foundation of China (No. 52006156) and the Hubei Provincial Natural Science Foundation of China (No. 2019CFA024, No. 2018CFB317).

REFERENCES

Ameli, A., Turunen-Saaresti, T., and Backman, J. (2016). Numerical Investigation of the Flow Behavior Inside a supercritical CO2 Centrifugal Compressor. Doi: 10.1115/GT2016-57481.

Behafarid, F., and Podowski, M. (2016). Modeling and Computer Simulation of Centrifugal CO2 Compressors at Supercritical Pressures. *Journal of Fluids Engineering*, 138, doi: 10.1115/1.4032570.

Brun, K., Friedman, P., and Dennis, R. (2017). *Fundamentals and Applications of Supercritical Carbon Dioxide (sCO2) Based Power Cycles*. Duxford: Woodhead Publishing.

Chen, H., Zhuge, W., Zhang, Y. and Liu, H. (2019). Effect of Compressor Inlet Condition on Supercritical Carbon Dioxide Compressor Performance. Doi: 10.1115/GT2019-90647.

Dostal, V., Hejzlar, P., and Driscoll, M. J. (2006). High-Performance Supercritical Carbon Dioxide Cycle for Next-Generation Nuclear Reactors. *Nuclear Technology*, 154, pp. 265-282.

Japikse, D. (1996).*Centrifugal compressor design and performance*. Wilder: Concepts ETI, Inc.

Lettieri, C., Baltadjiev, N., Casey, M., and Spakovszky, Z. (2014). Low-Flow-Coefficient Centrifugal Compressor Design for Supercritical CO2. *Journal of Turbomachinery*, 136, doi: 10.1115/1.4026322.

Lee, J,, Lee, J. I., Ahn, Y. and Yoon, H. (2012) Design Methodology of Supercritical CO2 Brayton Cycle Turbomachineries. Doi: 10.1115/GT2012-68933.

Liu, Z., Luo, W., Zhao, Q., Zhao, W., and Xu, J. (2018). Preliminary Design and Model Assessment of a Supercritical CO2 Compressor. *Applied Sciences*. 8(4), doi:10.3390/app8040595.

Ma, C., Wang, W., Wu, J., and Dai, L. (2018). Analysis of Unsteady Flow in a Supercritical Carbon Dioxide Radial Compressor Stage. Doi: 10.1115/ICONE26-82183.

Pecnik, R., Rinaldi, E., and Colonna, P. (2012). Computational Fluid Dynamics of a Radial Compressor Operating with Supercritical CO2. *Journal of Engineering for Gas Turbines and Power*, 134, doi: 10.1115/1.4007196.

Romei, A., Gaetani, P., and Persico, G. (2022). Computational Fluid-Dynamic Investigation of a Centrifugal Compressor with Inlet Guide Vanes for Supercritical Carbon Dioxide Power Systems. *Energy*, 225(7), doi:10.1016/j.energy.2022.124469.

Reyes-Belmonte, M. A., Sebastián, A., Romero, M., and Gon-zález-Aguilar, J. (2016). Optimization of a Recompression Supercritical Carbon Dioxide Cycle for an Innovative Central Receiver Solar Power Plant. *Energy*, 112, pp. 17-27.

Shao, W., Yang, J., Wang, X. and Ma, Z. (2020). A Real Gas Throughflow Method for the Analysis of SCO2 centrifugal compressors. Proceedings of the Institite of Mechanical Engineers, Part C: Journal of Mechanical Engineering Science, 234(10), doi: 10.1177/0954406220902188.

Yari, M. (2012). A Novel Cogeneration Cycle Based on A Recompression Supercritical Carbon Dioxide Cycle for Waste Heat Recovery in Nuclear Power Plants. *International Journal of Exergy*, 10, pp. 346-364.

Zhang, H., Li, Y., Chen, Z., Su, X. and Yuan, X. (2019). Multi-fidelity model based optimization of shaped film cooling hole and experimental validation. *International Journal of Heat and Mass Transfer*, 132, pp. 118-129.